Hindawi
Science and Technology of Nuclear Installations
Volume 2022, Article ID 7129092, 21 pages
https://doi.org/10.1155/2022/7129092

Research Article

Verification of the Efficacy of Passive Autocatalytic Recombiners in a Typical Pressurized Water Reactor under a Station Blackout Condition

Daegwang Hong,[1] Donghyun Cho,[1] Jinwoo Kim,[1] Aya Diab ,[1,2] and Cigdem Cildag[1]

[1]*KEPCO International Nuclear Graduate School, Ulsan, Republic of Korea*
[2]*Faulty of Engineering, Ain Shams University, Cairo, Egypt*

Correspondence should be addressed to Aya Diab; aya.diab@gmail.com

Received 4 May 2021; Accepted 29 January 2022; Published 12 March 2022

Academic Editor: Alexander Zulauf

The presence of a stable stratified gas cloud inside the containment near or at the flammability limit may lead to deflagration or even detonation which may challenge the containment and cause a radioactive material release into the environment. To mitigate this risk, a number of approaches have been proposed, for example, containment inerting or venting and use of passive autocatalytic recombiners or igniters. However, for these measures to be effective, a thorough analysis of the hydrogen dispersion and associated phenomena is indispensable during the design phase as well as the mitigation phase during a severe accident. In this work, a MAAP analysis is performed to assess the hydrogen risk in a typical pressurized water reactor (PWR) containment. An extended station blackout (SBO) was chosen as an initiating event given its high contribution to the core damage frequency. RCS depressurization and external injection are mitigation techniques implemented consecutively to extend the coping capability of the plant for the extended SBO scenario. A sensitivity study is performed to select the combination of timing and flow rate that generate the most severe case for the "in-vessel phase of hydrogen generation." Subsequently, a number of passive autocatalytic recombiners (PARs) were implemented to mitigate the hydrogen risk during the first three days of the accident. The Shapiro diagram is used to assess the flammability condition of the containment atmosphere based on MAAP analysis. The results show that the gas mixture composition is acceptable in the majority of the containment compartments and only marginally acceptable in the cavity. Even under the conservative conditions of the accident, the simulation results confirmed the sufficiency of recombiners alone without igniters in the low hydrogen concentration zones, while for compartments close to the sources, additional mitigation may be needed.

1. Introduction

In any hypothetical severe accident, oxidation of the fuel cladding at the high temperatures of the core may occur leading to production and release of hydrogen into the containment building. When hydrogen mixes with the oxygen present in the containment atmosphere, flammable gas pockets may form locally even in presence of steam. Such a condition may threaten the containment integrity, and hence hydrogen dispersion has become an important safety concern especially after the Three Mile Island accident and was recently revived as a potential risk after the Fukushima Daiichi accident.

The presence of a stable stratified gas cloud inside the containment near or at the flammability limit may lead to deflagration or even detonation which may result in breaching the containment and releasing radioactive material into the environment. To mitigate this risk, a number of approaches have been proposed, for example, containment inerting or venting and use of passive autocatalytic recombiners or igniters. However, for these measures to be effective, a thorough analysis of the hydrogen dispersion and associated phenomena is indispensable during the design phase as well as the mitigation phase during a severe accident.

Generally, for such class of problems, the thermal hydraulic response of the plant can be analyzed using lumped parameter (LP) codes or computational fluid dynamics (CFD) codes. A number of codes have been specially developed by the nuclear industry for multidimensional containment analyses, such as GOTHIC [1, 2], GASFLOW [3], and TONUS [4] and notably the severe accident analysis codes, for example, RELAP/SCDAP [5, 6], MAAP [7, 8], MELCOR [9–11], and ASTEC [12–14]. Other general-purpose commercially available CFD codes have been also explored for nuclear safety simulations including containment analyses [15], for example, by Heitsch et al. [16], Prabhudhardwadkar et al. [17], and Filippov et al. [18]. Application of commercial CFD codes may be challenged by the high computational overhead at the containment scale. Additionally, they may require additional models (e.g., condensation in the presence of noncondensables [19]) before they are capable of analyzing this class of problems, as evident by the studies conducted using ANSYS-CFX [20–22], ANSYS-FLUENT [19, 23, 24], and OpenFOAM [25].

In this work, the Modular Accident Analysis Program (MAAP) code is performed to assess the hydrogen risk in a typical pressurized water reactor (PWR) containment and evaluate the efficacy of implementing passive autocatalytic recombiners (PARs) in the various compartments of the containment building. MAAP is an integral lumped parameter (LP) code owned and licensed by the Electric Power Research Institute (EPRI) and can be used to simulate the thermal hydraulic response of the primary system, secondary system, and containment during severe accidents. MAAP can simulate the key phenomena in a severe accident particularly core heat-up, melting, and corium relocation using a variety of fuel states as shown in Figure 1. Five node types are available to describe the core degradation as the accident progresses. Four types (IGTYP) represent the normal fuel pin, collapsed fuel pin, and thickened fuel pin configurations. Two additional types are available: one for a nearly empty node and one for a fully molten node.

Moreover, it is equipped with the necessary models to estimate the reactor vessel thermal and mechanical response as a result of the progression of the accident. MAAP can also account for direct containment heating, molten corium concrete interactions, fission products release, aerosol transport, and deposition. And more importantly, it can model fuel oxidation, hydrogen generation, and dispersion. Hydrogen combustion models are also available to assess the extent of localized burning that could occur in the containment for severe accidents. Furthermore, it is possible to assess the hydrogen mitigation strategy using passive autocatalytic recombiners (PARs) which is necessary for hydrogen risk analysis. Thus, MAAP can be used to evaluate the survivability envelope for such conditions or for fast and efficient scooping simulations.

2. Methodology

Considering the implications of hydrogen risk in nuclear power plants, a severe accident scenario leading to significant hydrogen generation is selected. The Korean Advanced Power Reactor (APR1400) is used as a sample plant. Based on the APR1400 Probabilistic Risk Assessment (PRA) report, a station blackout (SBO) is among the highest contributors to core damage frequency and is therefore selected for this work. To evaluate the effectiveness of APR1400 Severe Accident Management Guidelines (SAMGs) during a postulated severe accident from a hydrogen risk perspective, a numerical simulation is conducted via the Modular Accident Analysis Program (MAAP). It is worth noting that the simulation scope is limited to the in-vessel hydrogen generation phase, that is, the ex-vessel hydrogen generation during a later phase as a result of molten corium concrete interaction is not considered in the current study.

First, a MAAP input deck is prepared for the base case scenario of APR1400 undergoing an extended SBO without any mitigation action for a better understanding of the plant response. Next, a model including two mitigation actions, RCS depressurization and external injection into the primary side, is developed. To examine the effectiveness of SAMG for APR1400, it is necessary to identify the scenario-based uncertainties (depressurization timing, injection timing, and rate) as well as phenomena-based uncertainties (effect of models and correlation parameters). A sensitivity analysis is used to find the worst-case scenario from a hydrogen risk perspective. The results of these simulations help identify the conditions that will lead to the highest possible hydrogen production during the in-vessel phase of the selected accident scenario. Subsequently, this condition is used to assess the efficacy of the implementation of PARs in the various containment compartments.

2.1. Basic Plant Model. In this analysis, MAAP 5.04 was used with full package of user's manual and sample parameter files. To initiate MAAP, a parameter file with the plant-specific design data should be selected. The nodalization provided for Zion plant with two loops, each connecting to the reactor pressure vessel via a hot leg and two cold legs, is selected to represent the APR1400 model. The plant model includes the primary side, the secondary side, and the containment model. The reactor core is modelled using 7 rings (channels) and 13 rows as shown in Figure 2. The first row of nodes represents the core support plate and the second row represents the lower gas plenum and lower tie plate, while the last row of nodes represents the upper gas plenum and upper tie plate. To monitor the hydrogen distribution in the containment, the containment nodalization needs to be considered. The plant parameter file provides the containment nodalization shown in Figure 3. Four compartments are modelled: the cavity (①, 95–97 ft), the annular compartment (④, 100–120 ft), the lower compartment (②, 138–163 ft), and the upper compartment (③, 182–270 ft). The hydrogen mole fraction (NFH2RB) can be extracted for each compartment to evaluate the hydrogen concentration before and after hydrogen mitigation system activation.

2.2. Fluidic Device. To properly simulate the safety injection system of APR1400, the fluidic device was implemented in the MAAP model. This fluidic device controls the mass flow

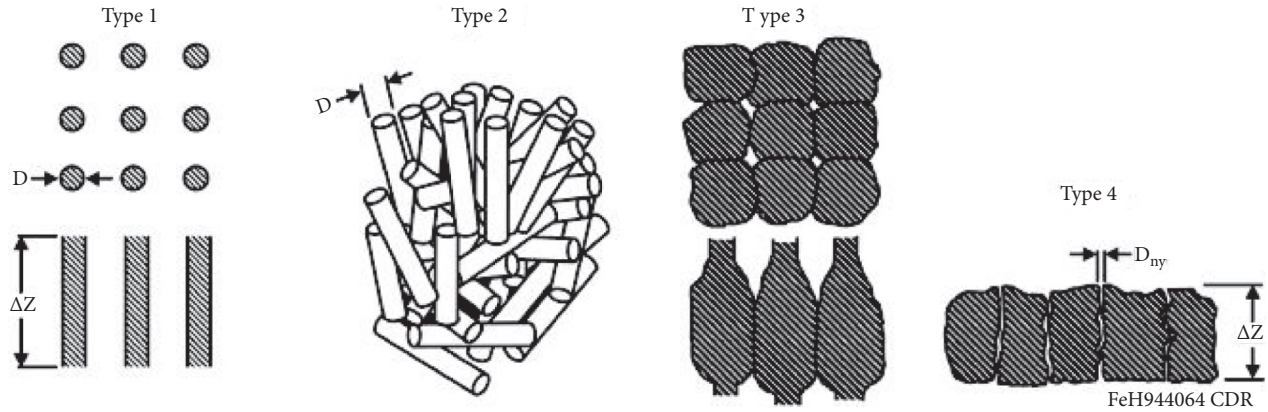

Figure 1: MAAP core geometry during melt progression.

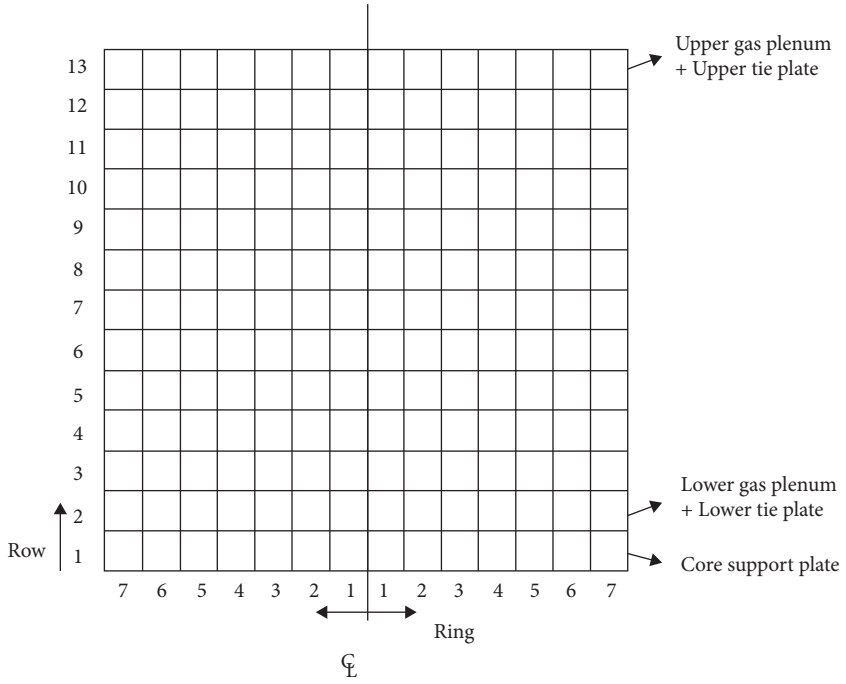

Figure 2: Core nodalization.

rate from the safety injection tanks (SITs). Its innovative design enables the core cooling to be maintained for a longer time duration under Large Break Loss of Coolant Accident (LBLOCA) conditions [26]. Because of the fluidic device of APR1400, the SIT initially delivers a high mass flow rate through both the stand pipe and the control port. However, when the water level of the SIT decreases below the stand pipe, water is injected only through the control port and the flow experiences a high swirl. This high swirl causes high resistance and hence a low injection flow rate.

Based on the experimental results of the SIT fluidic device [27], when the SIT level decreases from 8.8 m to 5.2 m, the SIT injection flow is turned down and the flow rate is reduced, i.e., when the water level reaches about 60% of the initial water level.

To match the experimental SIT performance, the accumulator flow rate in MAAP code was tested by modeling a large break loss of coolant accident (LBLOCA). To match the SIT fluidic device design, the pressure drop in the accumulator line due to the elbows, valves, etc. was modelled by adjusting the loss coefficient (FKLOSSACUM). FKLOSSACUM is set to 100 in MAAP input file to reduce the accumulator flow rate when the mass of the accumulator reaches 60% as shown in Figure 4. The initial flow rate is high (~1000 kg/sec), which decreases over time until the turndown point. When the accumulator mass decreases to 60% of the initial mass, the flow rate is abruptly decreased to the low flow. Subsequently, the low flow rate drops slowly from ~300 to 100 kg/sec over ~140 seconds.

2.3. PAR Implementation. The Hydrogen Mitigation System (HMS) of APR1400 is designed to accommodate the hydrogen production from 100% active fuel clad metal-water

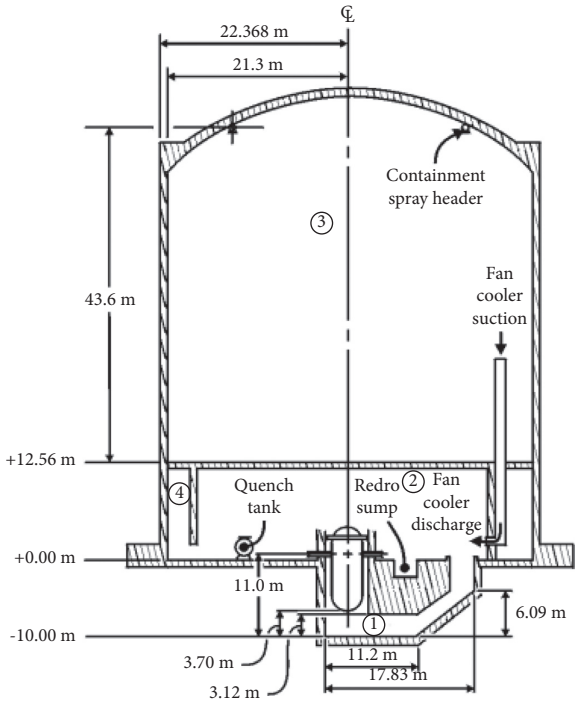

Compartment ID	Description
①	Cavity
②	Lower Compartment
③	Upper Compartment
④	Annular Compartment

Figure 3: Containment nodalization.

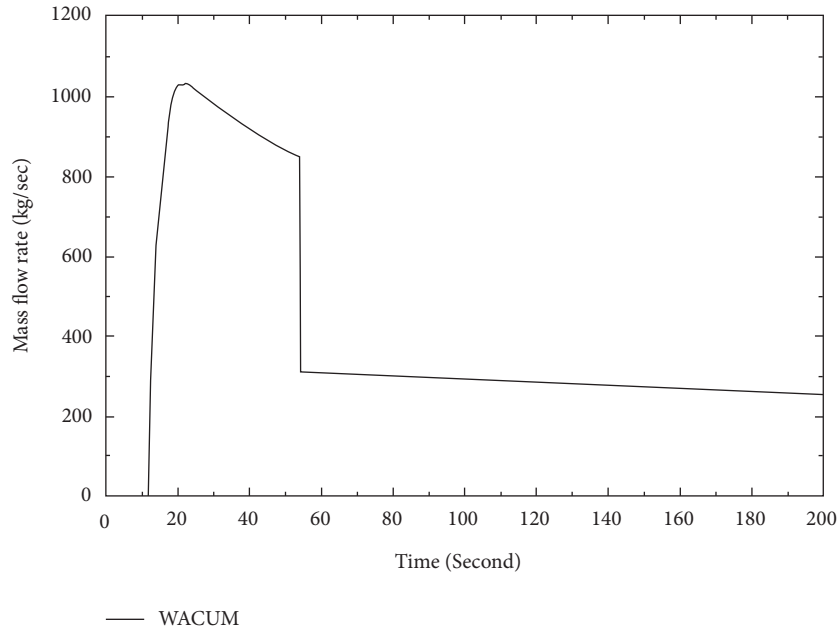

Figure 4: Simulated SIT mass flow rate.

reaction and limit the containment average hydrogen concentration to 10% in accordance with 10 CFR 50.34 (f). The HMS is designed such that the global hydrogen concentration will be below 5% by volume and the local hydrogen concentrations for containment volumes away from the hydrogen source can be maintained below 10% by volume [26]. In the event the local concentrations in any of the containment compartments or small rooms exceed 10% by volume near the hydrogen source [28], the resulting mixture should be either nondetonable (e.g., via steam inerting or oxygen depletion) or a detonation in the region will not result in a threat to containment integrity.

APR1400 is fitted with both hydrogen igniters and passive autocatalytic recombiners (PARs). The latter provides the means of controlling the global hydrogen concentration in the containment, while the former controls the local hydrogen concentration. Since PARs are self-actuated and require no electric power, they will be readily available

under the extended station blackout condition without any operator action. Accordingly, only the PARs will be considered; hydrogen mitigation with igniters will not be credited for the SBO scenario under investigation.

In high pressure sequences with a cycling relief valve, e.g., PORV, the PARs are required to maintain the hydrogen concentration in the containment below 10% by volume. Accordingly, PARs are distributed in APR1400 containment building such that the overall average concentration will be maintained below this limit. APR1400 uses thirty Korea Nuclear Tech (KNT) PARs in three sizes (small, medium, and large); the details of which are summarized in Table 1. To model APR1400 HMS, the PARs are distributed throughout the containment with reference to SKN units 3 and 4 according to the description provided in Chapter 6 of the final safety analysis report (FSAR), which summarizes the details of the actual construction and operation [26]. These locations are determined based on equipment specifications and piping proximity, as well as inspection and maintenance accessibility. The MAAP input file was prepared to reflect the actual APR1400 HMS (PAR model, quantity, and location) as closely as possible.

Of the PAR types available in MAAP 5.04, SIEMENS PAR was the closest to KNT PAR used in APR1400. Six SIEMENS PAR types are available. Type 2 (PAR SIEMENS FR90/1–150), type 3 (PAR SIEMENS FR90/1–320), and type 5 (PAR SIEMENS FR90/1–750) were chosen based on capacity (recombination rate) as the small, medium, and large PAR scales, respectively. According to Table 1, the recombination rates at 4.0 v/o H_2 for KNT PARs are 0.2 g/s, 0.4 g/s, and 0.9 g/s for the small, medium, and large scales, respectively. Another important parameter characteristic to the PAR operation is the start-up time (TDHPAR) which is the time needed for the system to warm-up before the PAR can be fully functional. In the parameter file, the recommended value is 5–10 minutes based on reference [29]. Therefore, 300 seconds is selected as TDHPAR, which is also the default value in the parameter file. A sensitivity study was performed with TDHPAR = 0 s, 300 s, and 1200 s, but the impact on the results was insignificant.

A user-defined PAR model is allowed in MAAP code, and the user can specify the details of the PAR model using the parameter file to match as closely as possible the specifications of KNT PARs such as capacity, start-up time, resolution and operable range, and limiting depletion rate, as well as location and quantity. Table 2 provides a summary of the items described in MAAP to reflect the characteristics of KNT PARs based on SKN units 3 and 4 Final Safety Analysis Report (FSAR). The cavity, the lower compartment, and the annular compartment includes five PAR units each, while the upper compartment is fitted with 15 PAR units. The specific location of each PAR unit is listed in Table 3 based on the APR1400 DCD document (Section 6.2.5in [26]). More details regarding PAR distribution are listed in Table 4.

2.4. Scenario Selection. According to the APR1400 PRA study [28], a station blackout (SBO + LOOP) is considered being the highest contributor to the core damage frequency (CDF) with a 5.11×10^{-7}/yr frequency and 39.4 as shown in Figure 5. This scenario is therefore selected for being highly probable and capable of producing significant amounts of hydrogen. Specifically, a representative sequence of events for this scenario with a 1.03×10^{-8}/yr frequency and 89.5 cumulative contribution is selected. The selected scenario provides a conservative accident progression assuming that the SBO is initiated by a loss of offsite power (LOOP) event along with a concurrent failure of both EDGs and loss of all alternate AC power sources. Accordingly, all active systems including safety systems are inoperable. The scenario also assumes failure of secondary heat removal via the turbine-driven auxiliary feed water pumps (TDAFWPs) and the failure of offsite power recovery within 72 hours as shown in Figure 6. It is worth noting that the RCP seal applied to the latest APR1400 design is the Westinghouse's KSB type F designed to maintain the integrity for 72 hours even in a high-temperature of 573 K (572°F) and high-pressure of 16 MPa (2335 psia) environment [26], and therefore, no seal leakage is assumed in this analysis.

During a transient in which leakage rate from RCS is a little or nothing, the decay heat is removed by secondary side heat transfer. However, since the AC power is not recovered until battery depletion, MSSVs continue to release the pressure until the SGs are depleted. When the SGs dry out, the natural circulation stops and heat removal is no longer possible. The RCS pressure will rapidly increase until the PORV opening set point is reached; at which point, the RCS inventory is continuously discharged and the core starts to uncover, ultimately leading to fuel damage.

After selecting the scenario and preparing the plant model with the necessary modifications, a base case SBO scenario was conducted with all safety systems unavailable except the fluidic device. For the base case, no mitigation strategy is implemented (i.e., no depressurization or external injection). To determine the plant response under the accident conditions, important system parameters and performance metrics are monitored such as the time for the first core relocation, vessel breach, and hydrogen generation.

2.5. Accident Mitigation. When the SBO occurs, the operators are required to act in accordance with Emergency Operating Procedure (EOP) with the main focus to recover the AC power. Without the inclusion of the Diverse and Flexible Coping Strategies (FLEX) and given the assumptions of the selected sequence, depletion of secondary and primary cooling water is inevitable, and as the SGs dry out, the connection with the ultimate heat sink is lost. Consequently, natural circulation ceases and hence the core temperature will rise until the plant transitions into the Severe Accident Management Guidance (SAMG) as the core exit temperature reaches the SAMG entry condition at 649°C.

In SAMG, there are seven mitigation strategies: RCS depressurization, injection into the SGs, injection into the RCS, injection into the containment, mitigation of fission product release, control of containment condition, and hydrogen control. In this study, the first and third mitigation strategies are implemented. The RCS is depressurized by

Table 1: PAR characteristic for SKN units 3 and 4.

Company	Korea Nuclear Technology (KNT)
Type	Catalytic
Quantity (for each unit)	(i) Large: 16 (including 8 PARs for DBA) (ii) Medium: 10 (including 8 PARs for DBA) (iii) Small: 4
Recombination rate (g/sec)	(i) Large: 0.9 at 4.0 v/o H_2, 2.0 at 8.0 v/o H_2 (ii) Medium: 0.4 at 4.0 v/o H_2, 1.0 at 8.0 v/o H_2 (iii) Small: 0.2 at 4.0 v/o H_2, 0.5 at 8.0 v/o H_2
Operable hydrogen concentration	(i) Above 2.0 v/o (initial) (ii) Above 0.5 v/o (continuous)
Material	(i) Housing: stainless steel (ii) Catalyst: Al_2O_3 + Pt coating

Table 2: Key input parameters for PAR.

Input	Description	References
INEWPAR = 1	Use new PAR model	
NFH2MN = 0.005	Limiting depletion rate of hydrogen volume fraction	SKN 3 and 4 FSAR (Section 6.2.5.2)
TDHPAR = 300.0	Start-up (or warm-up) time	Reference [30]
NFHSTB = 0.02	Minimum hydrogen volume fraction to achieve the start-up time	SKN 3 and 4 FSAR (Section 6.2.5.2)
ILAWPAR = 1	Recombination law for a recombiner (1) Use Siemens 98 law (2) Use Siemens 93 law	
NH2MAXSIEM = 0.08	Hydrogen fraction limiting the recombination rate for SIEMENS type PAR	SKN 3 and 4 FSAR (Section 6.2.5.2)
NH2STARTSIEM = 0.02	Minimum hydrogen fraction for cold starting for SIEMENS type PAR	
NH2STOPSIEM = 0.005	Minimum hydrogen fraction for hot ending for SIEMENS type PAR	

Table 3: PAR type, number, and location [26].

Compartment	Small PAR (type 2) *SIEMENS FR90/1-150*	Medium PAR (type 3) *SIEMENS FR90/1-320*	Large PAR (type 5) *SIEMENS FR90/1-750*
① Cavity	1	4	—
② Lower	1	2	2
③ Upper	1	—	14
④ Annular	1	4	—

manually opening the PORV for reactor vessel venting. And then, the external water is injected into the RCS using the FLEX portable equipment. Considering the accident conditions, only the impact of implementing PAR on hydrogen control will be investigated in this study without any consideration for hydrogen igniters.

The next step is to implement the external injection strategy by using FLEX equipment such as a fire truck. However, first, the injection location, injection flow rate, and injection timing need to be decided. Given that the goal is to assess the efficacy of the hydrogen mitigation strategy under an extended station blackout condition, operator actions should be chosen such that they lead to significant hydrogen production under the accident conditions. To maximize the hydrogen production, external water should be injected when the cladding temperature is as high as possible, while the geometry is still coolable to maintain the maximum available oxidation front between the zirconium (reactant) and the oxidizer (steam) and the injected water must be just enough to offset the thermal load posed by the decay heat. This bare minimum flow rate will guarantee that all the water will evaporate right after injection and hence produce the maximum amount of steam for maximum hydrogen production in the vessel. Using the energy balance and neglecting the sensible heat needed to change the water condition from subcooled to saturated liquid, the water flow rate can be calculated as follows:

$$\dot{Q}_{\text{decay}} = \dot{m} * h_{fg}, \tag{1}$$

where $\dot{Q}_{\text{decay}}$ is the decay heat, $\dot{m}$ is the injected mass flow rate, and h_{fg} is the latent heat.

Depending on the accident conditions, whether or not the depressurization is applied, the RCS pressure, the accumulated decay heat, the cladding temperature, and hence the latent heat of vaporization will change and accordingly the required flow rate will change. For typical accident conditions, at ~3–3.5 hours from the accident, this flow rate varies (~30–40 kg/s) at an RCS pressure of ~13–15.5 MPa and peak cladding temperatures of ~2700–3100 K.

2.6. Sensitivity Study to Maximize Hydrogen Generation. As mentioned earlier, the conditions that maximize hydrogen generation in the reactor vessel are high fuel

Table 4: PAR distribution details.

#PAR	Location	Capacity	Elevation (ft)	Compartment
1	IRWST vent stack area	Middle	97	①
2	IRWST vent stack area	Middle	97	①
3	IRWST vent stack area	Middle	97	①
4	IRWST vent stack area	Middle	97	①
5	In-core instrument tube chase	Small	120	④
6	Cavity upper chamber room	Small	95	①
7	Regenerative heat exchanger room	Small	146	②
8	Pressurizer compartment	Small	194	③
9	Pathway between annular and lower compartments	Middle	102	④
10	Pathway between annular and lower compartments	Middle	102	④
11	Pathway between annular and lower compartments	Middle	116	④
12	Pathway between annular and lower compartments	Middle	116	④
13	Pathway between annular and lower compartments	Middle	138	②
14	Pathway between annular and lower compartments	Middle	138	②
15	Steam generator room	Large	147	②
16	Steam generator room	Large	147	②
17	Steam generator room	Large	182	③
18	Steam generator room	Large	182	③
19	Upper compartment	Large	185	③
20	Upper compartment	Large	185	③
21	Upper compartment	Large	185	③
22	Upper compartment	Large	185	③
23	Containment dome area	Large	270	③
24	Containment dome area	Large	270	③
25	Containment dome area	Large	270	③
26	Containment dome area	Large	270	③
27	Containment dome area	Large	270	③
28	Containment dome area	Large	270	③
29	Containment dome area	Large	270	③
30	Containment dome area	Large	270	③

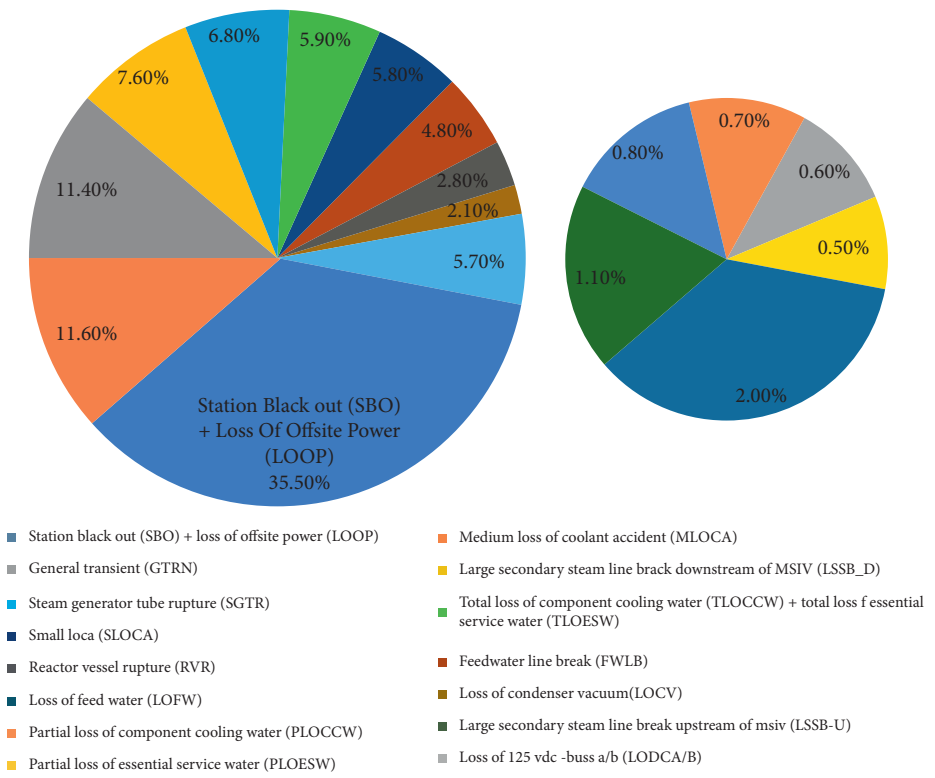

Figure 5: CDF contribution by initiating event.

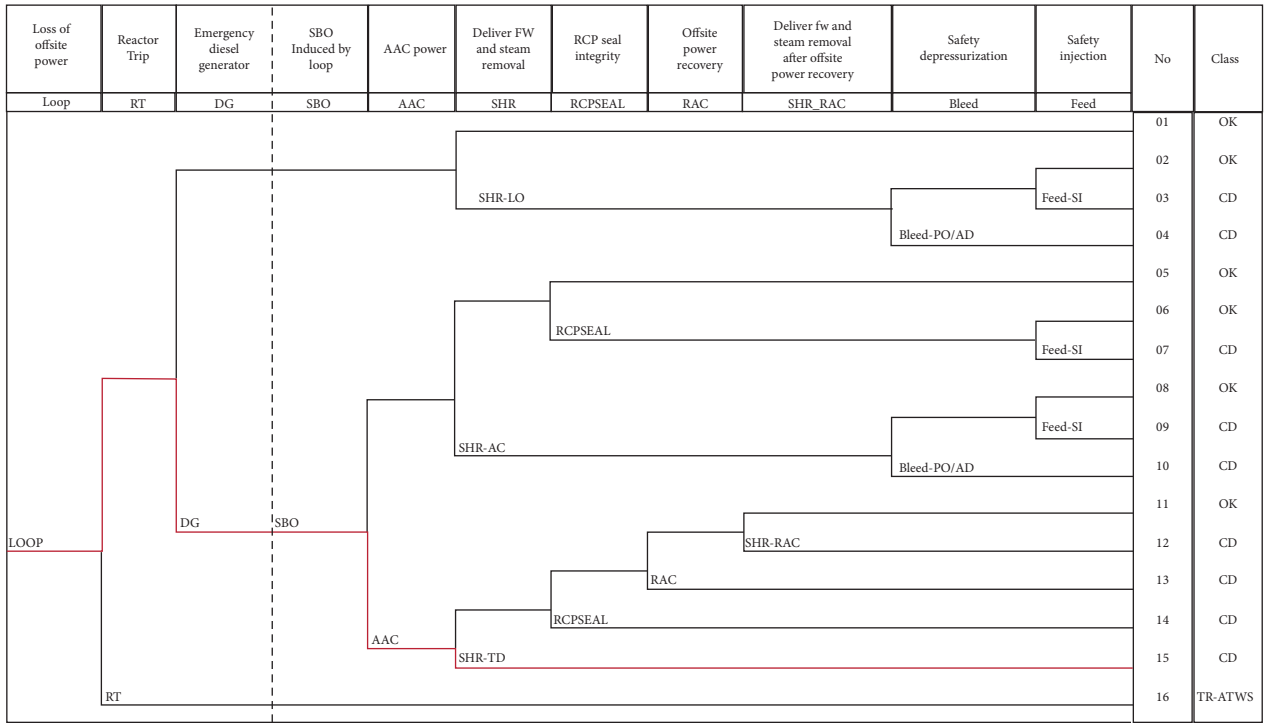

Figure 6: Level 1 event tree for the representative station blackout sequence.

temperature to initiate the reaction, a coolable core geometry for the reaction front, and a large amount of steam for zircaloy oxidation. However, there is a conflict between the former two factors, if the core temperature is higher than the melting temperature, the integrity of the core and hence a coolable geometry cannot be maintained. Furthermore, the amount of steam depends on the timing of external injection, which in turn depends on the depressurization timing.

To effectively model the injection, a sensitivity analysis was performed to decide the optimum timing for the external injection while maintaining a coolable geometry guided by the work of Park et al. [31] and Lil et al. [30] for scenario uncertainties: depressurization timing, external injection timing, and flow rate. In this sensitivity study, two depressurization timings were investigated: at core uncover and at the onset of core damage. Regarding the timing of external injection, five cases were studied: injection when the mass of SIT drops below ~0.5% of its initial mass, i.e., around its depletion time, and four more cases with some delay time (~1.5–4 hours). The external injection flow rate was also explored with full flow rate and 1/2 and 1/6 of the full flow rate.

It was determined that the external injection did not preserve the core geometry because of being relatively late. Accordingly, a sensitivity study is performed to analyze the effect of early external injection timing. Currently, the external water is injected when the mass of SIT drops below 0.5% of initial mass. In the sensitivity study, the injection condition was adjusted from 0.5% to 15%, 20%, 25%, 30%, and 45% with depressurization performed at the onset of core melting.

As for the phenomenological uncertainties, some of the core parameters need to be optimized. Consulting MAAP manuals, eleven parameters were somehow related to the oxidation and hence hydrogen generation. A brief description of the 11 MAAP parameters reviewed in this sensitivity study is shown in Table 5.

However, the sensitivity study (discussed in Section 3) revealed that only three main parameters (FAOX, TCLMAX, and EPSCUT) were the most impactful for hydrogen production. FAOX is the multiplier for the cladding outside surface area which reflects a phenomenological uncertainty. It is used in oxidation calculations once the core is uncovered to account for steam ingression after cladding rupture. The cladding rupture is calculated using the Larson–Miller material creep model. The model uses a critical temperature (TCLMAX) to identify creep. According to the Larson–Miller model, the cladding ruptures if it stays at TCLMAX for 36 seconds (0.01 hour). EPSCUT is the cutoff porosity below which the flow area and the hydraulic diameter of a core node are set to zero, i.e., the node is fully blocked. It is used to transition between a thickened fuel pin (IGTYP = 3) and crust (IGTYP = 4) configuration in the node. The smaller the value of EPSCUT, the more material relocation is necessary for a core node to become a crust node. The allowed ranges, default values, and used values of these parameters are summarized in Table 6.

3. Results and Discussion

3.1. System Response. As mentioned earlier, the accident scenario begins with the loss of offsite power, LOOP, along with SBO as initiating event. The pressure decreases instantaneously as shown in Figure 7(a) because the reactor is tripped when the SBO occurs. However, as shown in

Table 5: List of MAAP parameters reviewed in the sensitivity study.

Parameter	Range	Default	Description
LMCOL0 LMCOL1 LMCOL2 LMCOL3	48.0~54.0	53	(i) Collapse criterion parameters for a Larson–Miller-like functional dependence
EPSCUT	0.0~0.25	0.1	(ii) Cutoff porosity below which the flow area and the hydraulic diameter of a core node are zero
TCLMAX	100~3000 K	2500 K	(iii) Temperature that will lead to cladding rupture
FAOX	1.0~2.0	1.0	(iv) Multiplier for the cladding outside surface area
FGBYPA	0~1	1	(v) Flag to divert gas flows in the core to the bypass channel
TAUTO	750~1200 K	983 K	(vi)Autoignition temperature for hydrogen and carbon monoxide burns
TJBRN	900~1900 K	1060 K	(vii) Temperature of a H_2 jet entering a noninserted compartment which is sufficient to cause a local burn
DXHIG	−0.04~1	0.0	(viii) Offset H_2 and CO mole fraction for ignition of a flammable mixture
ENT0	0.025~0.060	0.045	(ix) Jet entrainment coefficient for the Ricou–Spalding correlation
EPSCU2	0.001~0.35	0.2	(x) Cutoff porosity below which the flow area and the hydraulic diameter of a collapsed core node
FZORUP	0.0~1.0	0.7	(xi) Minimum fraction of Zr that must be oxidized to keep the cladding intact if the cladding is at TCLMAX

Table 6: Key MAAP parameters impacting H_2 generation.

Parameter	MIN	MAX	Default	Used
FAOX	1.0	2.0	1.0	1.75
TCLMAX (K)	100	3000	2500	2750
EPSCUT	0.0	0.25	0.1	0.02

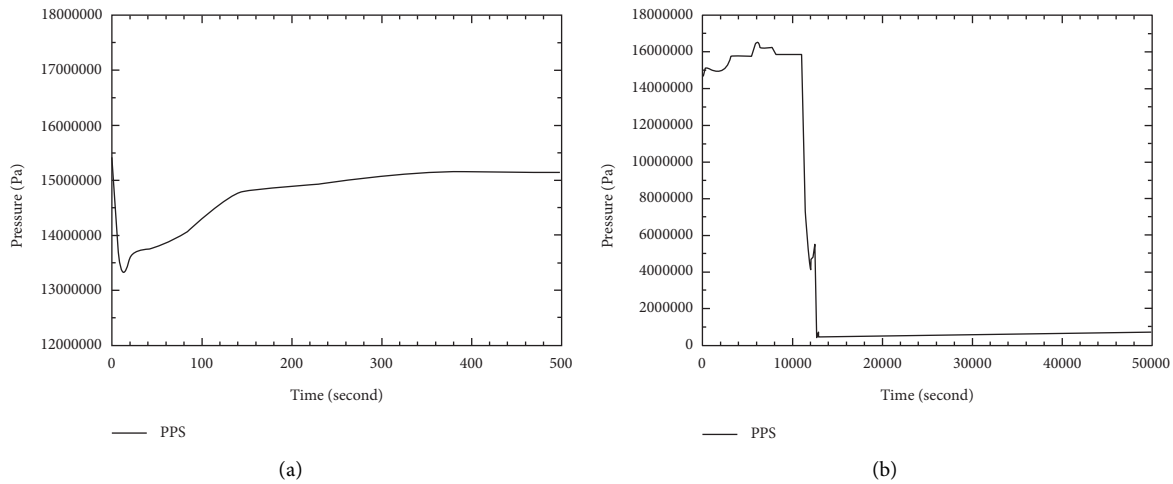

Figure 7: Pressure in primary system: (a) short term and (b) long term.

Figure 8, the pressure of the primary system gradually increases due to the loss of heat removal as the RCP pumps are stopped when the turbine is tripped and later due to the loss of natural circulation when the SGs dry out. As shown in Figure 9, the pressure on the secondary system also rises due to turbine valve closure when the turbine is tripped. As shown in Figure 10, due to the pressure rise, the safety valves of the primary and secondary systems operate cyclically to release some steam. Steam in the steam generator is released continuously through the secondary safety valves, but the auxiliary feedwater is not supplied. Therefore, eventually the SG is depleted at around 4000 seconds as shown in Figure 11 which illustrates the collapsed water level in the SG downcomer.

Given the loss of connection with the ultimate heat sink and the cyclic operation of the PORVs, the core uncovers at 7673 seconds as reported in Table 7, which causes the cladding to be oxidized and hydrogen to be generated as presented in Table 8. As shown in Figure 12, the temperature of the fuel cladding rises sharply because the upper part of the fuel is exposed to steam after core uncovery. At this time, the high-temperature cladding is oxidized and hydrogen is generated as shown in Figure 12. The total mass of hydrogen generated in the core is 741.36 kg for 3 days or 740.04 kg for 50,000 seconds as shown in Figure 12. As shown in Figure 12, most of the hydrogen is generated within about 50,000 seconds and rarely increased thereafter.

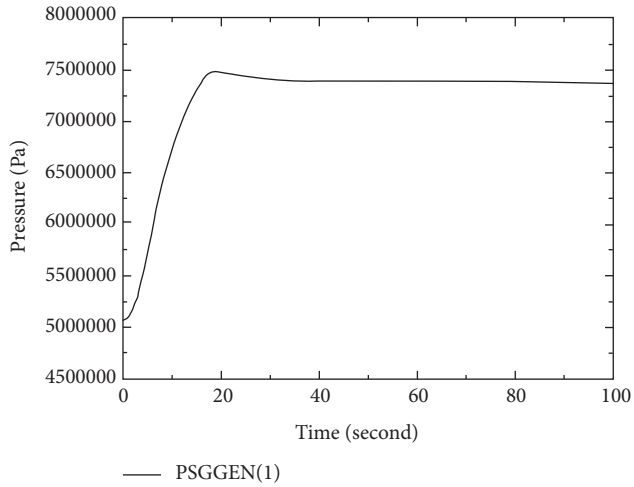

Figure 8: Pressure in the SG.

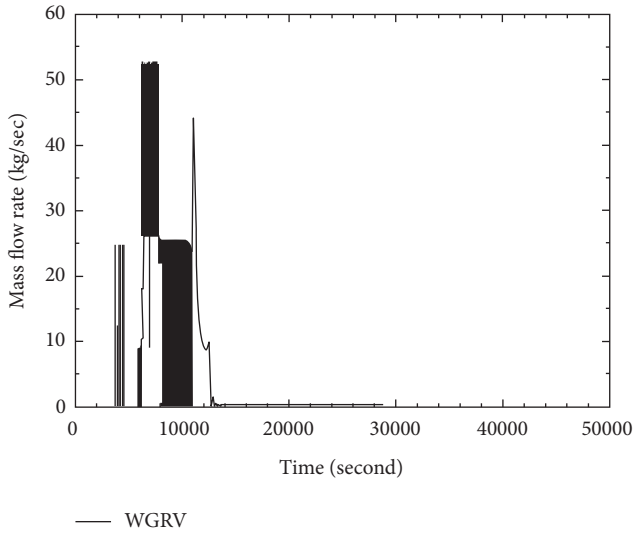

Figure 9: Gas flow rate of pressurizer through safety valves.

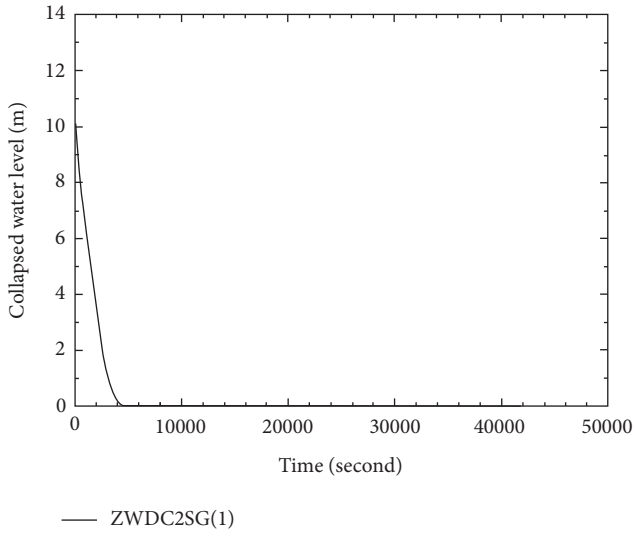

Figure 10: SG downcomer water level.

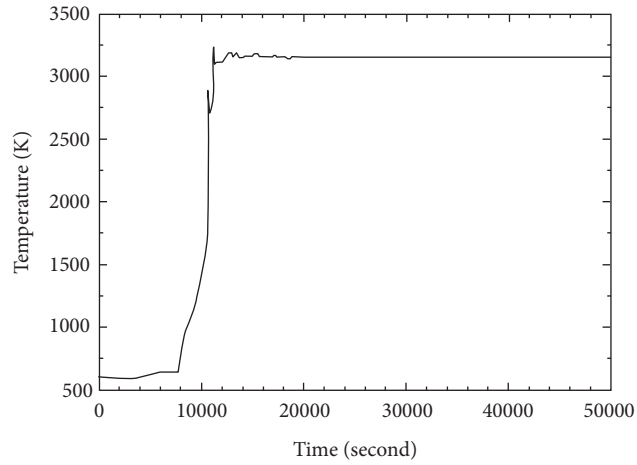

Figure 11: Hottest core node temperature.

Table 7: Summary of key events without PAR activation.

Event	Time (s)
Core uncovery	7673.09
Hot leg creep rupture	12,528.54
1st relocation to lower plenum	N/A
First vessel failure	N/A
Containment failure	99,925.36

As shown in Figure 7(b), when the operator opens PORVs at 11,000 seconds, the pressure drops sharply. Figure 9 shows the mass flow rate due to PORVs opening. As shown in Figure 7(b), the pressure increases temporarily due to accumulator injection at around 12,000 seconds even while PORVs are opened.

Figure 13 shows the mass flow rate of the accumulator. At 11,113 seconds, the core is damaged up to 50%. Figure 14 shows the mass flow rate of external injection. The pressure suddenly decreases again due to the hot leg creep rupture at 12,528 seconds as provided in Table 7. As shown in Figure 15, water is filled in the core and the core is covered by water since external injection is started. However, due to the hot leg creep rupture, steam which is generated from the core is continuously released into the containment building, which increases the pressure in the containment building until the design pressure limit is reached, breaching the containment building at 99,925 seconds as illustrated in Figure 16.

As shown in Figure 15, the core is filled with water by external injection and continuously replenished to overcome the phase change process due to decay heat. The generated steam oxidizes the cladding and produces hydrogen during the in-vessel phase of the accident.

3.1.1. Sensitivity Study. To maximize the in-vessel hydrogen production, three conditions need to be satisfied: the fuel temperature has to be as high as possible while maintaining a coolable geometry in the core in presence of a large amount of steam for zircaloy oxidation. The mitigation action should

Table 8: Key figures of merits without PAR activation.

Parameter	Value
Fraction of oxidized clad	83.66%
Total mass of H_2 in core	741.36 kg

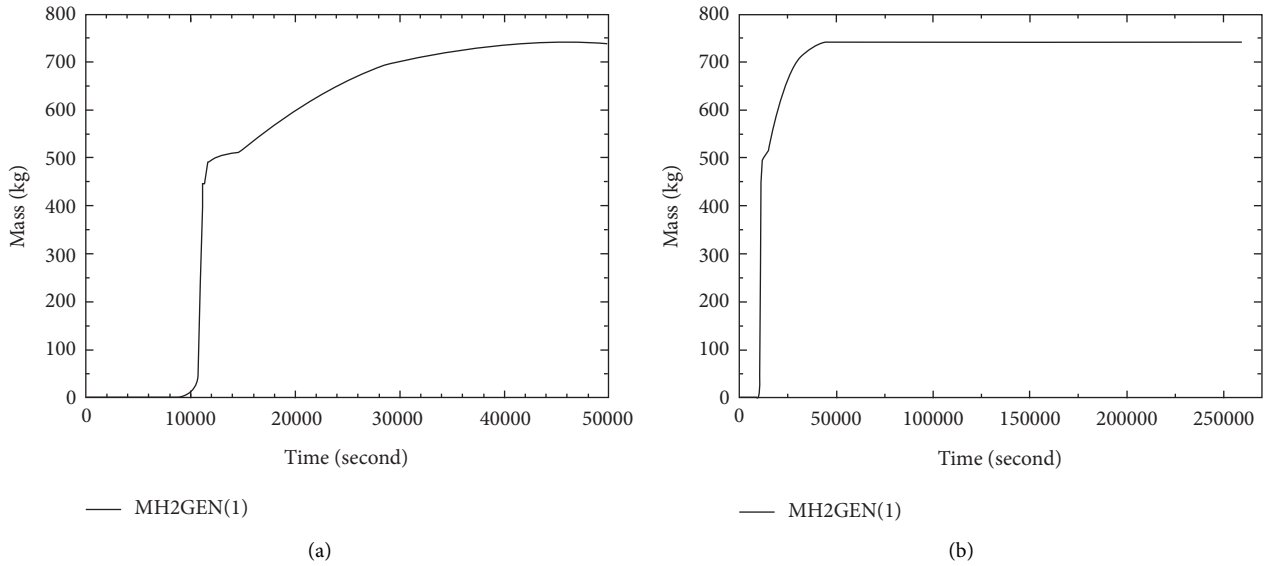

Figure 12: Total mass of hydrogen generated in core: (a) short term and (b) long term.

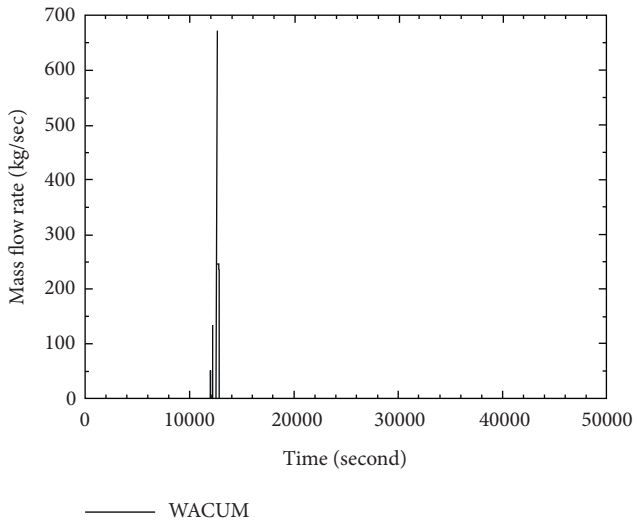

Figure 13: Accumulator mass flow rate.

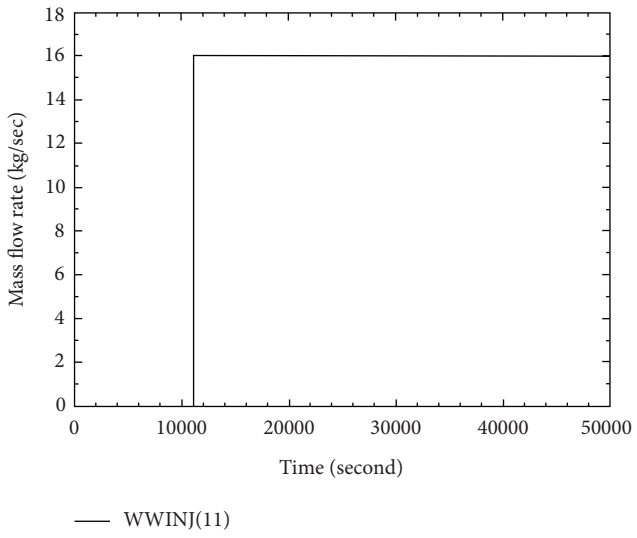

Figure 14: External injection mass flow rate.

not be too early to give a chance for enough decay heat to accumulate and raise the core temperature, but not too late to avoid the fuel from melting and hence lose the coolability. Furthermore, the amount of injected water should be just enough to offset the decay heat and turn into steam.

To select the proper conditions that will maximize the hydrogen production, a sensitivity study was conducted by changing the depressurization timing, as well as amount and timing of external injection.

Table 9 summarizes the results of changing the flow rate and time delay after SIT depletion. When the depressurization occurred at the core uncovery, the highest amount (400.84 kg) of hydrogen gas was produced with 1/6 of the full flow rate when injected just after SIT depletion. Any further time delay results in less hydrogen production, irrespective of the flow rate. When depressurization occurs at the onset of core damage, the amount of hydrogen produced is higher (469.36 kg) than that produced when depressurization occurs at core uncovery. With earlier depressurization, water from the SIT injection and external injection rushes quickly into the system to cool the core, which does not give a chance for the

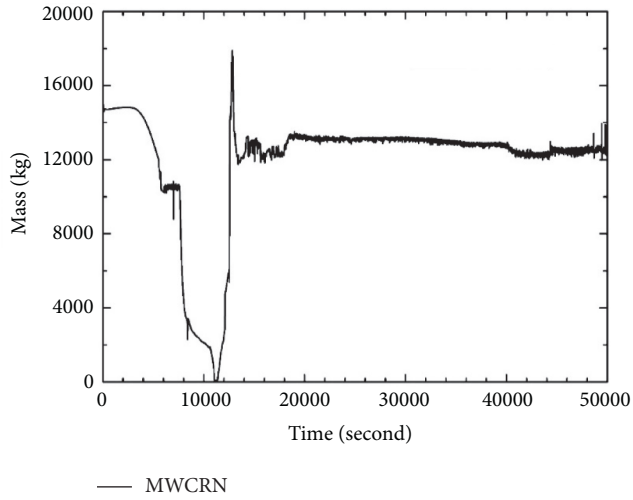

Figure 15: Mass of water in core.

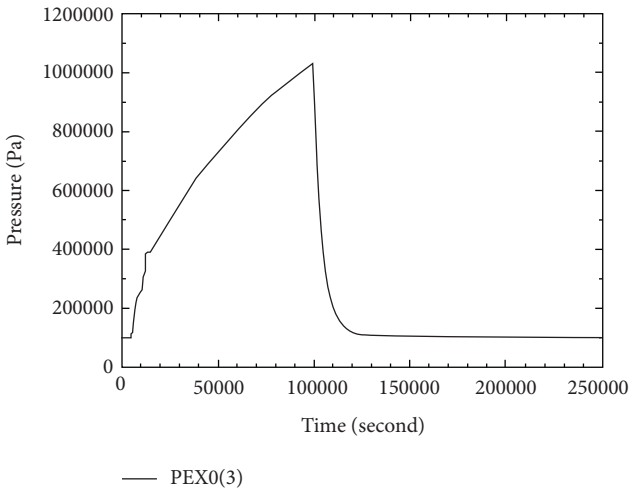

Figure 16: Pressure in containment.

temperature to rise and provide favorable conditions for the oxidation process.

When the system is depressurized at the onset of core damage with some delay in external injection, neither the amount of external water injection nor the time delay from SIT depletion seems to have an impact on the extent of oxidation as shown in Table 10. This can be attributed to the fact that, at those conditions, it was too late to preserve the coolable geometry. It is worth noting that, for the delayed external injections, the vessel was breached as the surge line underwent creep rupture. Under these conditions, the amount of steam remaining in the vessel after rupture would be small and similarly the oxidation front area for oxygen diffusion.

Accordingly, another sensitivity study is performed to analyze the effect of early external injection timing. Instead of injecting the external water after SIT depletion, the injection was initiated earlier when the SIT mass reached 15%, 20%, 25%, 30%, and 45% of its initial value. In this sensitivity study, depressurization was performed at the onset of core melting.

Table 11 illustrates how the depressurization at the onset of core melting along with earlier external injection is more influential in terms of hydrogen generation relative to depressurization at the time of core uncover with late external injection. The sensitivity study revealed that hydrogen generation is maximized when 1/6 of the full flow rate of the external injection was initiated when the mass of SIT drops below 45% of its initial mass. Under these conditions, the bare minimum flow rate the external injection is introduced at a time when the core temperature was high enough to satisfy the oxidation condition while geometry was still coolable but not too late to incur melting.

As shown in Table 12, among the 11 parameters, EPSCUT, TCLMAX, and FAOX impacted the hydrogen generation the most, with TCLMAX being the most influential parameter. When TCLMAX (the mean cladding rupture temperature) is raised, more hydrogen is generated since the integrity of the core geometry is guaranteed at higher temperature for longer time. In addition, it can be seen that the relationship with hydrogen generation is not linear, which confirms the need for the sensitivity study for MAAP parameters.

So far, the sensitivity study confirms that the hydrogen generation is maximized when depressurization is performed at the onset of core melting, i.e., at the first change in core configuration. In consideration of the mutual interaction of the three major MAAP parameters (EPSCUT, TCLMAX, and FAOX) and possible effect of depressurization timing, a sensitivity study was conducted according to the four possible combinations of these parameters. The results shown in Table 13 indicate the significance of only two parameters (TCLMAX and FAOX). It was confirmed that when those three parameters are simultaneously varied (one parameter at a time), hydrogen generation is greatly affected. In addition, the greatest amount of hydrogen was generated when depressurization is performed around the time of first change in core configuration as expected.

However, MAAP predicts that external water is injected at 17,731 seconds, when its initiation time is based on the SIT water level. This is later than the time of first relocation to the lower plenum (15,831 seconds); hence, vessel failure was inevitable since there is almost no water available for heat removal or for that matter, steam for hydrogen generation by external injection. This has led to the need to find the optimal external injection time and flow rate linking the injection timing with the progression of the core damage, rather than the condition of SIT water level. Accordingly, only two combinations of those parameters were performed in this study. The results of this sensitivity study are shown in Table 13.

Case 14 led to the highest amount of hydrogen generation and was therefore selected as the base case for following the sensitivity study of the external injection flow rate and injection time.

As mentioned in the previous sections, the condition of high hydrogen generation is when water is injected while high temperature and core geometry configuration are maintained. This sensitivity study was performed to find the timing of external injection considering relation between two contradictory factors (high temperature and coolable geometry). Core damage was calculated according to

Table 9: Effect of external injection flow rate and time delay (depressurization at core uncovery).

Ext. injection flow rate (kg/s)	Time delay from SIT depletion (s)				
	0	6000	9000	12,000	15,000
1/6 flow (6.25)	400.84 kg H_2	399.64 kg H_2	399.64 kg H_2	399.64 kg H_2	399.64 kg H_2
Half flow (18.75)	399.95 kg H_2	399.64 kg H_2	399.64 kg H_2	399.64 kg H_2	399.64 kg H_2
Full flow (37.5)	399.94 kg H_2	399.64 kg H_2	399.64 kg H_2	399.64 kg H_2	399.64 kg H_2

Table 10: Effect of external injection flow rate and time delay (depressurization at core melting).

Ext. injection flow rate (kg/s)	Time delay from SIT depletion (s)				
	0	6000	9000	12,000	15,000
1/6 flow (6.25)	469.36 kg H_2	469.36 kg H_2	469.36 kg H_2	469.36 kg H_2	469.36 kg H_2
Half flow (18.75)	469.36 kg H_2	469.36 kg H_2	469.36 kg H_2	469.36 kg H_2	469.36 kg H_2
Full flow (37.5)	469.36 kg H_2	469.36 kg H_2	469.36 kg H_2	469.36 kg H_2	469.36 kg H_2

Table 11: Effect of injection timing on H_2 generation (depressurization at core melting).

Ext. injection flow rate (kg/s)	Remaining SIT mass				
	45%	30%	25%	20%	15%
1/6 flow (6.25)	**504.74** kg H_2	501.81 kg H_2	501.60 kg H_2	497.99 kg H_2	496.07 kg H_2
Half flow (18.75)	463.17 kg H_2	469.86 kg H_2	470.24 kg H_2	471.20 kg H_2	471.35 kg H_2
Full flow (37.5)	461.00 kg H_2	469.69 kg H_2	469.92 kg H_2	470.72 kg H_2	473.86 kg H_2

fraction of nodes with degree of IGTYP 2 to IGTYP 5 (as illustrated in Figure 1) to monitor the core configuration status. The time was measured by core damage percentage, and external water was injected at each timing. The depressurization was performed at 11,000 seconds accordingly. The results of this sensitivity study is shown in Table 14).

To represent transition from a thickened pin type configuration to a node which begins to be part of the molten pool and crust, a specific fuel condition is identified by parameter IGTYP in terms of increasing damage. Table 15 and Figure 17 show the timings and core temperature distribution according to the core damage percentage calculated based on the core configuration status. It can be seen that the core is damaged in a short period of time (about 100 seconds) from 11,022 seconds.

According to the heat balance, the optimum flow rate of external injection was calculated as 32 kg/s. Guided by the work of Park et al. (2014), a sensitivity study was performed with the timing and flow rate of external injection as described in Table 16.

The most hydrogen generation case was case 21 (740.04 kg hydrogen). Although case 31 generated slightly more hydrogen, case 21 was chosen as the final result because case 21 has more preserved core geometry. Regarding MAAP parameters, FAOX, TCLMAX, and EPSCUT, they were set at 1.75, 2750 K, and 0.02, respectively. Also, depressurization was performed at 11,000 seconds, i.e., at the onset of core damage. The external injection flow rate that maximizes the hydrogen production is 16 kg/sec (half flow rate), and the timing of external injection corresponds to a 50% damaged core.

3.1.2. Hydrogen Distribution. To investigate the hydrogen distribution in the containment, the nodalization provided for the Zion plant is used and the hydrogen mole fraction is monitored as a function of time for the cavity, lower compartment, upper compartment, and annular compartment as the accident progresses. Consider the results shown in Figure 17; after hot leg creep rupture, hydrogen is released to the containment atmosphere due to the buoyancy and inertial effects. Since the flow resistance between compartments is different, the dispersion of hydrogen varies for each compartment. The upper compartment has more hydrogen than the others as illustrated in Table 17.

If injection is too late, the coolable geometry cannot be maintained, and hence the interfacial area for the zirconium-steam oxidation front is reduced. Alternatively, if injection is too early, the core is quenched and the temperature condition in the core is not favorable for oxidation. Steam is produced in the core at a rate that is proportional with the decay heat. When the water of the external injection reaches its saturation point, it changes into steam. In the event of a hot leg creep rupture, both steam and hydrogen are released from the vessel to the containment atmosphere; consequently, the hydrogen concentration drops due to dilution upon mixing with steam and air. After some time, however, the steam exchanges heat with the containment walls and condenses. Hence, the hydrogen concentration in the containment increases which explains the strong correlation between the steam mole fraction and the hydrogen mole fraction in Figure 18.

3.2. Flammability Limit. Tracking the progression of the containment mixture in the different compartments is very important since it can be used to detect the flammability condition. The Shapiro diagram shown in Figure 19 demonstrates that based on the averaged global concentrations, the mixture is outside the flammability range for each of the containment compartments. However, one should be quite

Table 12: Effect of MAAP parameters (phenomenological uncertainty).

Parameter	Range	Default	Value	H_2 mass (kg)	Variation (%)	Case#
LMCOL0*	48.0~54.0	53	48	448.34	−5.9	1
LMCOL1			50	460.70	−3.3	2
LMCOL2			52	473.49	−0.6	3
LMCOL3			54	475.91	−0.1	4
EPSCUT	0.0~0.25	0.1	0	486.97	2.3	5
			0.08	491.60	3.2	6
			0.16	481.56	1.1	7
			0.25	479.67	0.7	8
			0.02	**495.61**	**4.1**	**9**
			0.04	480.4	0.9	10
			0.06	490.79	3.1	11
TCLMAX	100~3000 K	2500 K	2000	341.06	−28.4	12
			2250	368.97	−22.5	13
			2750	**516.77**	**8.5**	**14**
			3000	498.08	4.6	15
FAOX	1.0~2.0	1.0	1.25	438.4	−7.9	16
			1.5	476.25	0.0	17
			1.75	**489.36**	**2.8**	**18**
			2	482.48	1.3	19
FGBYPA	0~1	1	0	462.74	−2.8	20
			0.25	462.74	−2.8	21
			0.5	476.25	0.0	22
			0.75	476.25	0.0	23
TAUTO	750~1200 K	983 K	750	476.25	0.0	24
			900	476.25	0.0	25
			1050	476.25	0.0	26
			1200	476.25	0.0	27
TJBRN	900~1900 K	1060 K	900	480.9	1.0	28
			1233	469.7	−1.4	29
			1566	471.4	−1.0	30
			1900	471.4	−1.0	31
DXHIG	−0.04~1	0.0	−0.04	476.25	0.0	32
			0.31	476.25	0.0	33
			0.65	476.25	0.0	34
			1	476.25	0.0	35
ENT0	0.025~0.060	0.045	0.04	475.66	−0.1	36
			0.045	476.25	0.0	37
			0.05	476.71	0.1	38
EPSCU2	0.001~0.35	0.2	0.15	470.17	−1.3	39
			0.2	476.25	0.0	40
			0.25	479.67	0.7	41
			0.3	473.74	−0.5	42
FZORUP	0.0~1.0	0.7	0.6	476.25	0.0	43
			0.65	476.25	0.0	44
			0.7	476.25	0.0	45
			0.75	476.25	0.0	46
			0.8	476.25	0.0	47

The bold values point to the case with maximum hydrogen production.

careful in assessing these results since they are based on a lumped parameter approach. Even though the containment may not undergo global detonation, the results may not exclude local detonations based on the local hydrogen concentrations which are not predicted by such lumped parameter code. In other words, the global concentrations reported by the code may mask local high hydrogen concentrations in excess of the flammability/detonation limits. This issue needs to be resolved by distributed parameter (CFD) codes, for example, FLUENT, OpenFOAM, or CUPID codes.

3.3. Results after PAR Implementation. Table 18 summarizes the time for key events during the accident progression after the PAR model is implemented and activated. The core uncovers at ~2.13 hrs, the hot leg experiences creep ruptures at ~3.48 hrs, and ultimately the containment fails at ~24 hrs. During the accident, 74.89% of the fuel has been oxidized yielding an in-vessel hydrogen generation of 663.67 kg, as shown in Table 19.

The generated hydrogen is released from the vessel right after hot leg creep rupture and mixes with the steam and other gases in the containment atmosphere. The mole

Table 13: Results of sensitivity study #5 (MAAP parameter, base case).

Depressurization time (sec)	EPSCUT	TCLMAX	FAOX	H_2 mass (kg)	Case#
10,850	0.02	2750	Default	510.61	1
	Default	2750	1.75	536.07	2
	0.02	Default	1.75	470.64	3
	0.02	2750	1.75	534.46	4
10,900	0.02	2750	Default	506.83	5
	Default	2750	1.75	523.21	6
	0.02	Default	1.75	461.72	7
	0.02	**2750**	**1.75**	**544.95**	**8**
10,925	0.02	2750	Default	504.37	9
	Default	2750	1.75	543.33	10
	0.02	Default	1.75	459.92	11
	0.02	2750	1.75	537.39	12
10,950	0.02	2750	Default	531.90	13
	Default	2750	1.75	530.30	14
	0.02	Default	1.75	457.29	15
	0.02	2750	1.75	516.91	16
11,000	0.02	2750	Default	526.41	17
	Default	2750	1.75	519.92	18
	0.02	Default	1.75	457.41	19
	0.02	2750	1.75	538.36	20
11,050	0.02	2750	Default	527.34	21
	Default	2750	1.75	531.24	22
	0.02	Default	1.75	461.05	23
	0.02	2750	1.75	543.11	24

The bold values point to the case with maximum hydrogen production.

Table 14: Result of sensitivity study #6 (base case without external injection).

Depressurization time (sec)	EPSCUT	TCLMAX	FAOX	H_2 mass (kg)	Oxidation (%)	Case#
9850	—	2750	1.75	492.44	55.57	1
	0.02	2750	1.75	487.41	55.00	2
10,350	—	2750	1.75	517.63	58.41	3
	0.02	2750	1.75	522.31	58.94	4
10,850	—	2750	1.75	546.57	61.68	5
	0.02	2750	1.75	544.79	61.47	6
10,900	—	2750	1.75	549.14	61.97	7
	0.02	2750	1.75	525.38	59.28	8
10,925	—	2750	1.75	543.02	61.27	9
	0.02	2750	1.75	534.93	60.36	10
10,950	—	2750	1.75	525.57	59.31	11
	0.02	2750	1.75	529.8	59.78	12
11,000	—	2750	1.75	529.61	59.76	13
	0.02	**2750**	**1.75**	**551.93**	**62.28**	**14**
11,250	—	2750	1.75	528.95	59.69	15
	0.02	2750	1.75	540.87	61.03	16
11,500	—	2750	1.75	513.85	57.98	17
	0.02	2750	1.75	523.9	59.12	18
11,750	—	2750	1.75	493.85	55.73	19
	0.02	2750	1.75	504.88	59.97	20
12,000	—	2750	1.75	495.55	55.92	21
	0.02	2750	1.75	504.84	56.97	22
12,500	—	2750	1.75	493.6	55.70	23
	0.02	2750	1.75	504.87	56.97	24
13,000	—	2750	1.75	493.71	55.71	25
	0.02	2750	1.75	504.86	56.97	26

The bold values point to the case with maximum hydrogen production.

fraction of the hydrogen in various compartments of the containment building can be seen in Figure 20 as the accident progresses over time with and without PAR activation. The lower compartment experiences the highest hydrogen concentration as a peak is observed shortly after the occurrence of creep rupture. After mixing with the

Table 15: Time and temperature distribution due to core damage.

Core damage (%)	Time	TCRHOT	TCLN (10)	TCLN (11)	TCLN (12)
2	10,712.07	2904.63	1188.90	1212.61	1240.69
5	11,022.86	2791.10	2947.34	2910.90	2802.80
10	11,063.00	2852.93	2873.68	2911.00	2911.00
20	11,103.05	3215.81	2795.75	2826.26	2832.83
50	11,113.06	3183.19	2787.10	2819.45	2876.16
60	11,133.09	3132.79	2768.05	2802.11	2687.49
70	11,263.13	3100.05	2870.40	2758.78	2854.08
80	11,604.11	3118.26	2911.00	2872.66	2860.10
90	21,259.88	3121.04	100.00	100.00	100.00

TCRHOT: maximum core temperature; TCLN (i): clad temperature in node i.

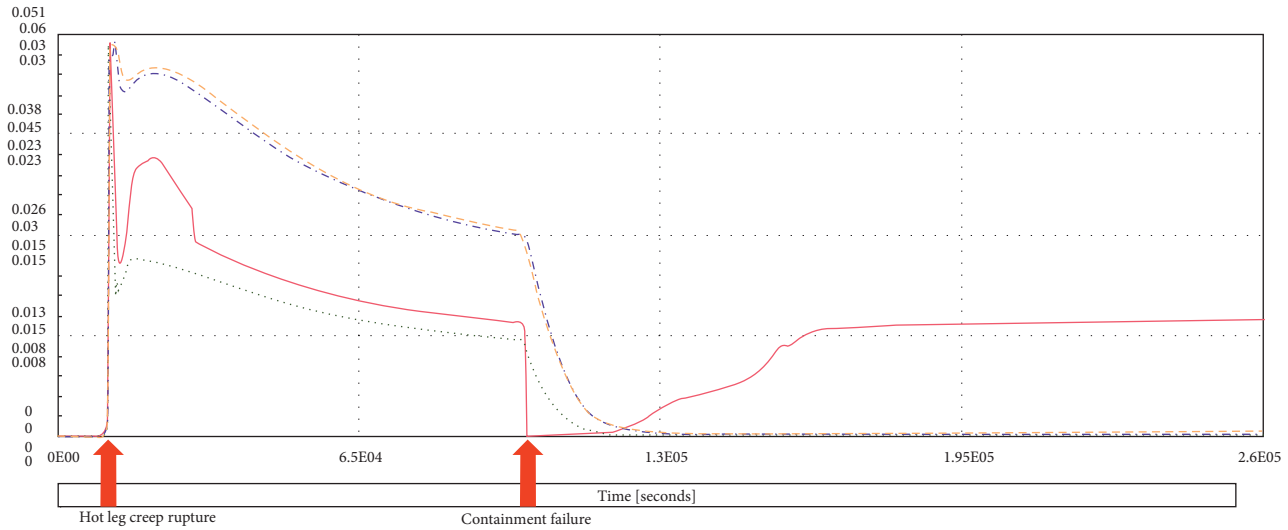

Figure 17: Hydrogen mole fraction in compartments: ① cavity (solid red), ② lower (dotted green), ③ upper (phantom blue), and ④ annular (dashed yellow).

Table 16: Result of sensitivity study #7 (timing and flow rate of external injection).

Flow rate	Time (sec)	Core damage (%)	H_2 mass (kg)	Oxidation (%)	Case#
5 kg/s	11,010	—	537.59	60.89	1
	10,712	2	547.96	61.83	2
	11,022	5	539.11	60.83	3
	11,103	20	549.88	62.05	4
	11,113	50	532.87	60.13	5
	11,133	60	532.39	60.07	6
	11,263	70	557.66	62.93	7
	11,604	80	542.86	61.26	8
10 kg/s	11,010	—	526.16	59.37	9
	10,712	2	455.05	51.35	10
	11,022	5	531.82	60.00	11
	11,103	20	671.19	75.74	12
	11,113	50	531.17	59.94	13
	11,133	60	537.09	60.60	14
	11,263	70	530.24	59.83	15
	11,604	80	544.1	61.40	16
16 kg/s	11,010	—	695.55	78.49	17
	10,712	2	449.00	50.66	18
	11,022	5	700.37	79.03	19
	11,103	20	520.66	58.75	20
	11,113	**50**	**740.04**	**83.51**	**21**
	11,133	60	519.90	58.67	22
	11,263	70	535.79	60.46	23
	11,604	80	650.91	73.45	24

Table 16: Continued.

Flow rate	Time (sec)	Core damage (%)	H_2 mass (kg)	Oxidation (%)	Case#
20 kg/s	11,010	—	535.03	60.37	25
	10,712	2	437.53	49.37	26
	11,022	5	520.59	58.74	27
	11,103	20	522.94	59.01	28
	11,113	50	511.51	57.72	29
	11,133	60	650.06	73.35	30
	11,263	**70**	**745.10**	**84.08**	**31**
	11,604	80	655.75	73.99	32
32 kg/s	11,010	—	537.22	60.62	33
	10,712	2	135.47	15.29	34
	11,022	5	528.08	59.59	35
	11,103	20	538.95	60.81	36
	11,113	50	502.86	56.74	37
	11,133	60	503.46	56.81	38
	11,263	70	522.45	58.95	39
	11,604	80	653.30	73.72	40

Table 17: Peak values of hydrogen mole fraction.

Hydrogen concentration	Cavity compartment	Upper compartment	Lower compartment	Annular compartment
Fraction (%)	0.050254 (5.025)	0.058634 (5.863)	0.029524 (2.952)	0.028944 (2.894)

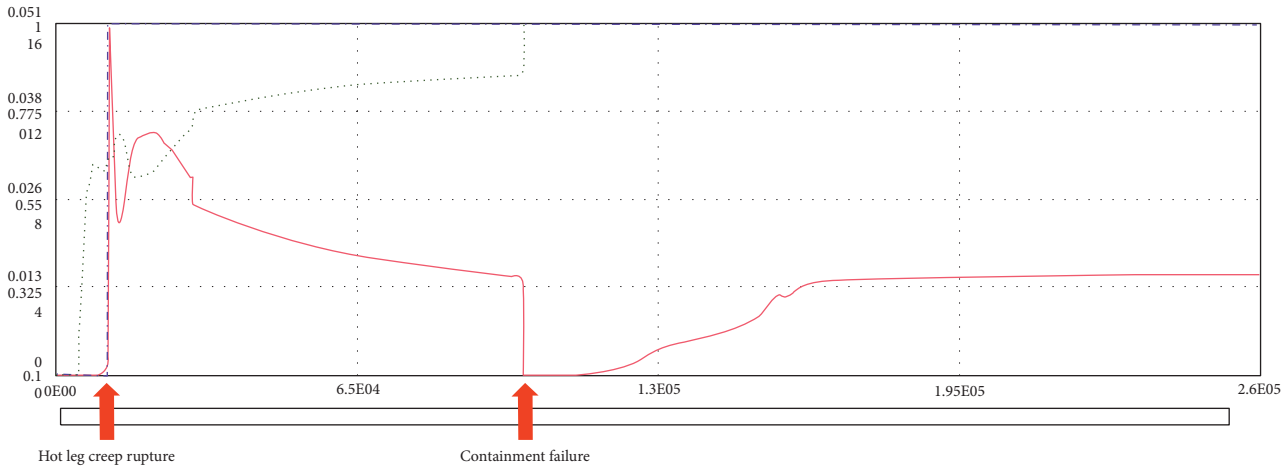

Figure 18: Steam mole fraction (dotted green), hydrogen mole fraction (solid red), and external injection mass flow rate for compartment ①.

containment environment, the molar fraction is seen to drop later during the accident. It is worth noting that the peak value of the hydrogen molar fraction is 5.8% which is less than the limit for the APR1400 containment building (10% in accordance with 10 CFR 50.34 (f)) and drops significantly with activation of PARs. However, this finding should be treated with care since the model used is a lumped-parameter model and the numbers reflect only globally averaged values. Even though the globally hydrogen concentration may be less than the threshold value, this does not preclude the possibility of having localized pockets of hydrogen with concentrations in excess of the safety limit.

As shown in Figure 21, PAR activation has been successfully implemented in the model. The results show that the upper compartment, ③, has the highest recombination rate since it has 14 large capacity PARs. However, the lower compartment, ②, has the highest hydrogen concentration as Table 20 indicates. The amount of recombined hydrogen in each compartment is also shown in Table 21. The lower compartment is fitted with 2 large, 2 medium, and 1 small recombiners, but the results show that the number or capacity of implemented PARs in this compartment may not be sufficient. Although the location of PARs is not exact, it is expected that it might be better to install more PARs in this compartment or simply replace some PARs with higher

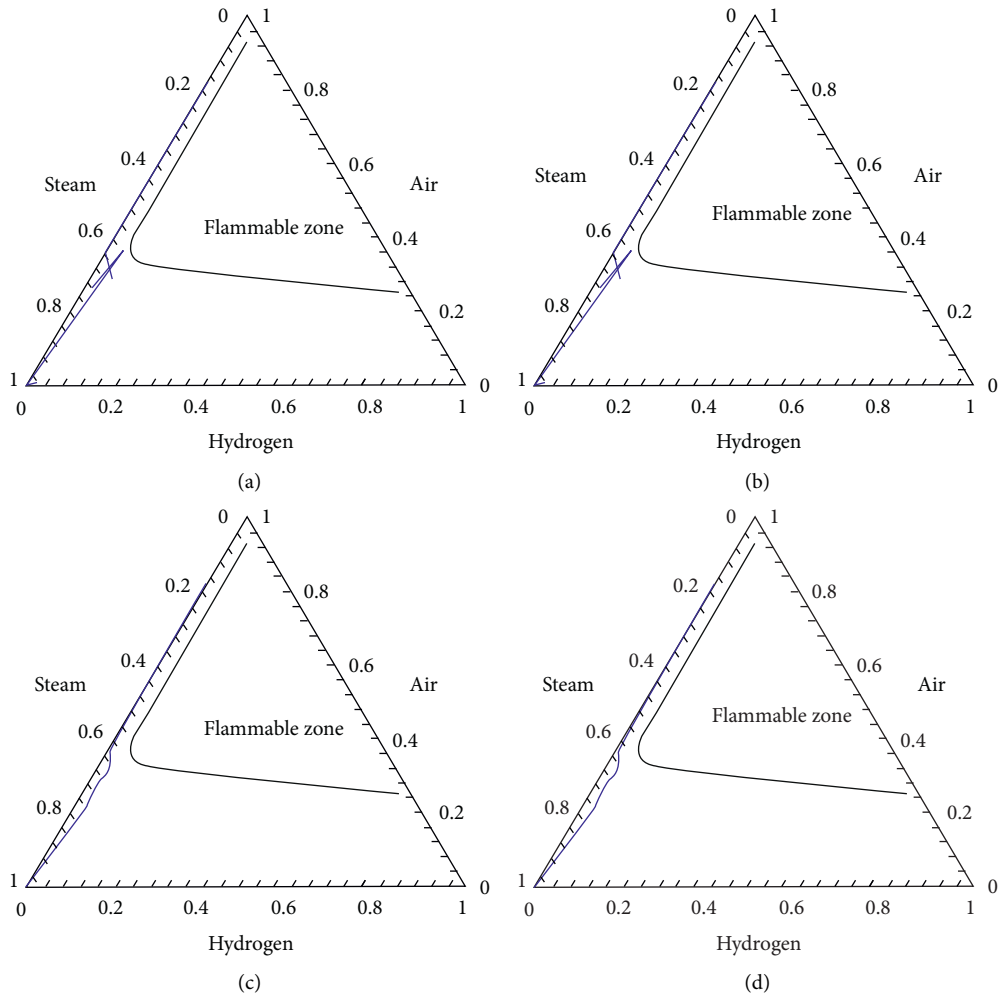

Figure 19: Shapiro diagram for each compartment. (a) Cavity compartment, ①; (b) lower compartment, ②; (c) upper compartment, ③; and (d) annular compartment, ④.

Table 18: Time of key events with PAR activation.

Event	Time (s)
Core uncovery	7673.09
Hot leg creep rupture	12,541.14
Containment failure	86,750.69

Table 19: Key figures of merits with PAR activation.

Parameter	Value
Fraction of oxidized clad	74.89%
Total mass of H_2 in core	663.67 kg

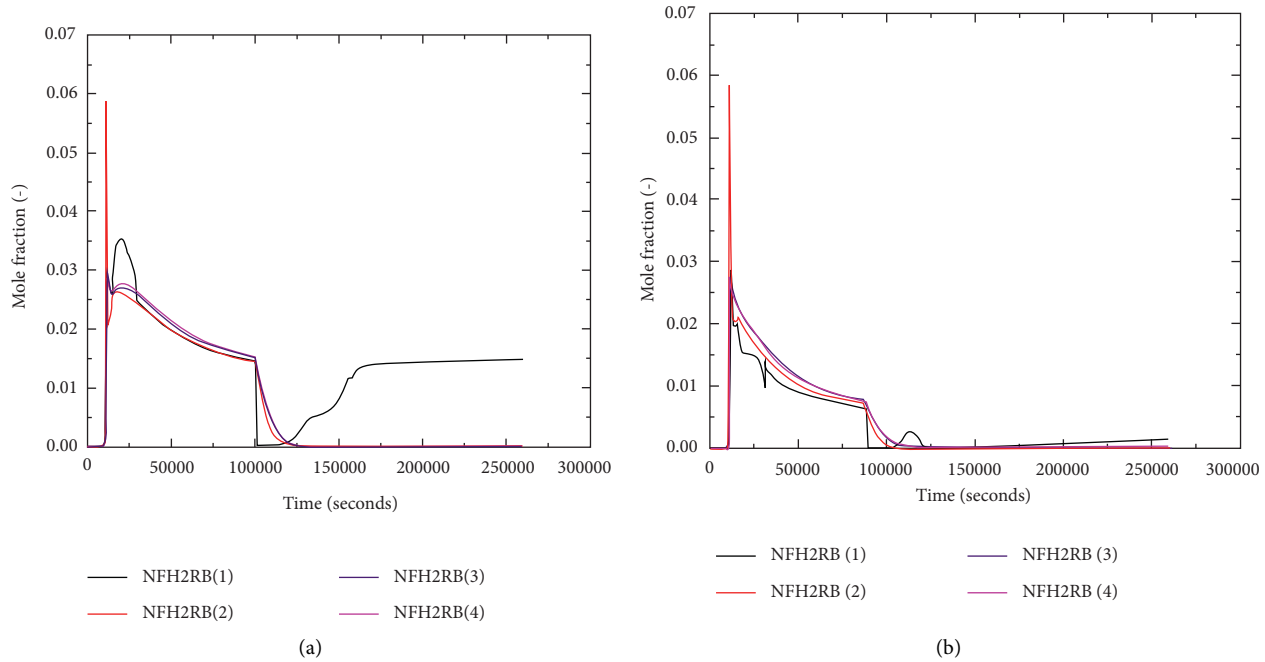

Figure 20: Mole fraction of hydrogen for each compartment: (a) without PAR modeling and (b) with PAR modeling.

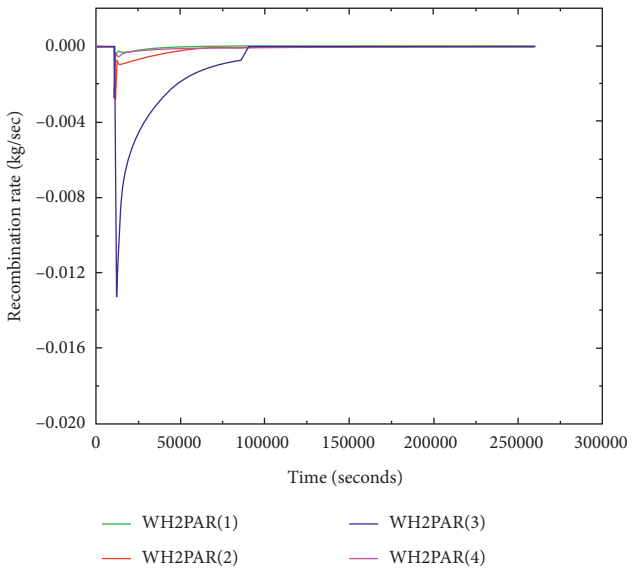

Figure 21: Recombination rate of PARs in each compartment.

Table 20: Peak value of hydrogen mole fraction with PAR modeling.

NFH2BRN (1)	NFH2BRN (2)	NFH2BRN (3)	NFH2BRN (4)
0.046809	0.058309	0.028462	0.027958
4.681%	5.831%	2.846%	2.796%

Table 21: Total mass of recombined hydrogen (kg H_2) with PAR modeling.

Total	MH2PAR (1)	MH2PAR (2)	MH2PAR (3)	MH2PAR (4)
266.924	7.983	31.196	216.9714	10.774

capacity ones. This may be necessary to limit the local hydrogen concentrations and hence eliminate the associated risk. However, it is worth noting that the resolution of a lumped parameter code is inherently limited and a more detailed and highly resolved simulation (e.g., using a CFD code) for the cavity may be needed (Table 21).

4. Conclusions

MAAP analysis was performed to assess the hydrogen risk in containment. SBO concurrent with LOOP was chosen as an initiating event based on the APR1400 PRA study. RCS depressurization and external injection are SBO mitigation techniques implemented consecutively in this scenario. The scenario was simulated using MAAP 5.04, and a sensitivity study was performed to find out the conditions that maximize the hydrogen generation during the in-vessel phase of the severe accident. Subsequently, the impact of PARs on hydrogen risk mitigation during the first three days of the chosen scenario is investigated by monitoring the hydrogen fraction in the various compartments of APR1400 containment building. The Shapiro diagram was used to assess the hydrogen risk based on the flammability limit as the accident progresses. The MAAP results confirmed that the gas mixture in each of the containment compartments remained outside the flammability range. The beneficial effect of recombiners after activation of the PAR model was also established especially for areas with low hydrogen concentration. However, for the cavity compartment, the hydrogen concentration was marginally acceptable. Given the inherent limitation of lumped parameter codes, the results of MAAP may not confirm the exclusion of possible local concentrations in excess of the flammability limit, which necessitates the obvious demand for a CFD

calculation with high spatial resolution for accurate prediction of hydrogen dispersion and transport.

Data Availability

The data used to support the findings of this study may be available from the corresponding author upon request.

Conflicts of Interest

The authors declare that there are no conflicts of interest regarding the publication of this paper.

Acknowledgments

This work was supported by the 2021 Research Fund of the KEPCO International Nuclear Graduate School (KINGS), Republic of Korea.

References

[1] M. Andreani and D. Paladino, "Simulation of gas mixing and transport in a multi-compartment geometry using the GOTHIC containment code and relatively coarse meshes," *Nuclear Engineering and Design*, vol. 240, no. 6, pp. 1506–1527, 2010.

[2] M. Andreani, R. Kapulla, and R. Zboray, "Gas stratification break-up by a vertical jet: simulations using the GOTHIC code," *Nuclear Engineering and Design*, vol. 249, pp. 71–81, 2012.

[3] P. Roy, J. R. Travis, J. R. Travis, W. Baumann, and G. Necker, "Analyses of containment experiment with GASFLOW II," in *Proceedings of the Tenth International Topical Meeting on Nuclear Reactor Thermal Hydraulics, NURETH-10*, Seoul, South Korea, October 2003.

[4] S. Kudriakov, F. Dabbene, E. Studer et al., "The TONUS CFD code for hydrogen risk analysis: physical models, numerical schemes and validation matrix," *Nuclear Engineering and Design*, vol. 238, no. 3, pp. 551–565, 2008.

[5] R.-J. Park, S.-B. Kim, and H.-D. Kim, "Evaluation of the RCS depressurization strategy for the high pressure sequences by using SCDAP/RELAP5," *Annals of Nuclear Energy*, vol. 35, no. 2, pp. 150–157, 2008.

[6] R.-J. Park, S.-B. Kim, S.-W. Hong, and H.-D. Kim, "Detailed evaluation of coolant injection into the reactor vessel with RCS depressurization for high pressure sequences," *Nuclear Engineering and Design*, vol. 239, no. 11, pp. 2484–2490, 2009.

[7] J. W. Park and W.-C. Seol, "Considerations for severe accident management under extended station blackout conditions in nuclear power plants," *Progress in Nuclear Energy*, vol. 88, pp. 245–256, 2016.

[8] B. C. Lee, J. H. Jeong, and M. G. Na, "Effects of accident management strategy on the severe accident environmental conditions," *Annals of Nuclear Energy*, vol. 33, no. 1, pp. 13–21, 2006.

[9] S. Seo, Y. Lee, S. Lee, H.-Y. Kim, and S. J. Kim, "Effectiveness and adverse effects of reactor coolant system depressurization strategy with various severe accident management guidance entry conditions for OPR1000," *Journal of Nuclear Science and Technology*, vol. 52, no. 5, pp. 695–708, 2015.

[10] Y. J. Lee, W. J. Choi, S. W. Seo, H. Y. Kim, and S. J. Kim, "Development of safety injection flow map associated with target depressurization for effective severe accident management of OPR1000," *Journal of Nuclear Science and Technology*, vol. 53, pp. 1–11, 2016.

[11] Y. Lee, W. Choi, and S. J. Kim, "Efficacy assessment of independent severe accident mitigation measures in OPR1000 using MELCOR code," *Journal of Nuclear Science and Technology*, vol. 54, no. 1, pp. 89–100.

[12] S. Šadek, D. Grgić, and Z. Šimić, "Application of ASTEC, MELCOR, and MAAP computer codes for thermal hydraulic analysis of a PWR containment equipped with the PCFV and PAR systems," *Science and Technology of Nuclear Installations*, vol. 2017, p. 16, Article ID 8431934, 2017.

[13] P. Matejovic, M. Barnak, M. Bachraty, L. Vranka, and Z. Tuma, "VVER-440/V213 long term containment pressurization during severe accident," *Nuclear Engineering and Design*, vol. 377, Article ID 111145, 2021.

[14] P. Matejovic, M. Barnak, M. Bachraty, and L. Vranka, "ASTEC applications to VVER-440/V213 reactors," *Nuclear Engineering and Design*, vol. 272, pp. 245–260, 2014.

[15] B. L. Smith, "Assessment of CFD codes used in nuclear reactor safety simulations," *Nuclear Engineering and Technology*, vol. 42, no. 4, 2010.

[16] M. Heitsch, R. Huhtanen, Z. Téchy et al., "CFD evaluation of hydrogen risk mitigation measures in a VVER-440/213 containment," *Nuclear Engineering and Design*, vol. 240, no. 2, pp. 385–396, 2010.

[17] D. M. Prabhudharwadkar, K. N. Iyer, N. Mohan, S. S. Bajaj, and S. G. Markandeya, "Simulation of hydrogen distribution in an indian nuclear reactor containment," *Nuclear Engineering and Design*, vol. 241, no. 3, pp. 832–842, 2011.

[18] A. S. Filippov, S. Y. Grigoryev, O. V. Tarasov, and T. A. Iudina, "CFD simulation of PANDA and MISTRA cooler tests of ERCOSAM-SAMARA project," in *Proceedings of the 2014 22nd International Conference on Nuclear Engineering, ICONE22*, Prague, Czech Republic, July 2014.

[19] D. C. Visser, M. Houkema, N. B. Siccama, and E. M. J. Komen, "Validation of a FLUENT CFD model for hydrogen distribution in a containment," *Nuclear Engineering and Design*, vol. 245, pp. 161–171, 2012.

[20] G. Zschaeck, T. Frank, and A. D. Burns, "CFD modelling and validation of wall condensation in the presence of non-condensable gases," *Nuclear Engineering and Design*, vol. 279, pp. 137–146, 2014.

[21] M. Punetha and S. Khandekar, "A CFD based modelling approach for predicting steam condensation in the presence of non-condensable gases," *Nuclear Engineering and Design*, vol. 324, 2017.

[22] B. Schramm, J. Stewering, and S. Martin, *Validation of a Simple Condensation Model for Simulation of Gas Distributions in Containments with CFX*.

[23] A. Dehbi, F. Janasz, and B. Bell, "Prediction of steam condensation in the presence of noncondensable gases using a CFD-based approach," *Nuclear Engineering and Design*, vol. 258, pp. 199–210, 2013.

[24] J.-D. Li, "CFD simulation of water vapour condensation in the presence of non-condensable gas in vertical cylindrical condensers," *International Journal of Heat and Mass Transfer*, vol. 57, no. 2, pp. 708–721, 2013.

[25] R. Thiele, "Modeling of Direct Contact Condensation with OpenFOAM," MS Thesis, Royal Institute of Technology, Stockholm, Sweden, 2010.

[26] KEPCO/KHNP, *APR1400 Design Control Document Tier2, Chapter 6: Engineered Safety Features", APR1400-K-X-FS-14002-NP*, 2014.

[27] I. Ju, N. Choi, J. Jeong, B. Cho, and C. Song, *Performance Verification Test for APR1400 Fluidic Device, KAERI/TR-2836/2004*, 2004.

[28] KEPCO/KHNP, *APR1400 Design Control Document Tier2, Chapter 19: Probabilistic Risk Assessment and Severe Accident Evaluation, APR1400-K-X-FS-14002-NP*, 2014.

[29] M. Klauck, E.-A. Reinecke, S. Kelm, N. Meynet, B. Ahmed, and H.-J. Allelein, "Passive auto-catalytic recombiners operation in the presence of hydrogen and carbon monoxide: experimental study and model development," *Nuclear Engineering and Design*, vol. 266, 2014.

[30] L. Liu, M. Zhang, and J. Deng, *Analysis of RCS Depressurization Effects on Containment Temperature for Qinshan Phase II Nuclear Power Plant*, ICONE22-30649, 2014.

[31] J. W. Park and W.-C. Seol, "Considerations for severe accident management under extended station blackout conditions in nuclear power plants," *Progress in Nuclear Energy*, vol. 88, pp. 245–256, 2016.